Materials
Advances

PAPER
M. Soorani *et al.*
Structural effects of incorporating Cu⁺ and Cu²⁺ ions
into silicate bioactive glasses using molecular dynamics
simulations

Check for updates

Structural effects of incorporating Cu$^+$ and Cu^{2+} ions into silicate bioactive glasses using molecular dynamics simulations

M. Soorani, [ID] * E. Mele [ID] and J. K. Christie [ID]

Copper oxide containing bioactive glasses have drawn attention because of their unique properties as biomaterials for targeted tissue engineering applications. This is due to their ability to act as stimulants for new tissue formation. In the present manuscript, we aim to study the structure and properties of copper incorporated bioactive glass 45S5 using molecular dynamic simulations using newly parameterized interaction potentials for Cu$^+$–O and Cu^{2+}–O oxides. The role of copper oxides in 45S5 glasses was elucidated by studying a series of glasses with compositions 46.1 mol% SiO$_2$, 26.9 mol% CaO, 24.4 mol% Na$_2$O, and 2.6 mol% P$_2$O$_5$ in which CuO (10, 15, and 20 mol%) was progressively substituted for Na$_2$O. The local environment of Cu$^+$ and Cu^{2+} ions within the glasses was explored and the ratio was calculated theoretically. The findings indicate that both Cu$^+$ ions with a three-fold coordination and Cu^{2+} ions coordinated by six oxygen atoms participate in the silica network as network modifiers. The impact of Cu$^+$ and Cu^{2+} ions on the overall glass network connectivity was likely to be small. The ratio of Cu$^+$: Cu$_{total}$ has been found to increase with an increase in the content of CuO in the structure of the studied glasses. In the computational study of the glasses, the network connectivity was used to predict their bioactivity. From our study, it was concluded that incorporating Cu$^+$ and Cu^{2+} ions in the structure of 45S5 glasses favours the bioactivity of these glasses.

1. Introduction

Copper (Cu) as a trace mineral has been investigated for its therapeutic potential in the human body since it is a necessary micro-nutrient in maintaining body haemostasis.[1,2] The amount of copper in humans depends on the gender, weight, and age.[3] An individual with a body weight of 70 kg has about 110 mg of copper.[4] Half of this amount is found in the bones and muscles while the rest is taken up by the skin, bone marrow, liver and brain.[5] Copper exists in its reduced (Cu$^+$ or cuprous) state inside cells.[6] This makes it a suitable cofactor in different biological processes such as energy metabolism and anti-oxidant activity. Trace metals like this are referred to as biologically active. Free copper ions are harmful and toxic to the cells and because of this reason, the uptake, distribution and haemostasis of copper are highly regulated.[7] Copper also plays an important role in the strength of skin, blood vessels, epithelial cells, and connective tissue, and participates in a wide variety of catalytic functions and molecular interactions throughout the body.[8] Copper and its compounds have mostly been studied for their efficacy against pathogenic bacteria,

microbes, viruses, and deadly fungal species.[9,10] Copper is an essential element in maintaining the production of hemoglobin, myeline, and melanin as well as in regulating the function of the thyroid gland and it acts as an antioxidant and neutralizes free radical damage.[8] Gene expression is also affected by copper-dependent enzymes.[11]

Copper at a low dose (in a range up to 8.66 mg kg^{-1}) is counted as an essential nutrient for the body.[12,13] An excess amount of this element, beyond the range of human tolerance, would be toxic to the biological tissue and even lethal at doses between 50 and 54.4 mg kg^{-1} due to the production of free radicals that cause toxicity and inflammatory effects.[13,14]

The invention of bioactive glass (BG) paved the way for modern biomaterial-oriented regenerative medicine.[15] From a tissue engineering point of view, BGs are excellent candidates in biological tissue regeneration and reconstruction as their physicochemical, mechanical, and biological features are comparable to those of biological tissue.[16,17] Moreover, as potent materials they can be drawn into different forms such as powder, fibers, and 3D porous scaffolds which enhance the regeneration process of both hard and soft tissues.[1] Cu-doped bioactive glasses (BGs) have also been studied for their applications in the synthesis of scaffolds in tissue engineering.[13] Cu-containing silicate-based glasses can be beneficial both in hard

Department of Materials, Loughborough University, Loughborough, LE11 3TU, UK. E-mail: M.Soorani@lboro.ac.uk

tissue and soft tissue engineering as they are anti microorganisms, and they can prevent infection. They are also capable of promoting cell differentiation. Silicate-based bioactive glasses (SiBGs) are amorphous materials which are highly reactive under physiological conditions.[18,19] SiBGs can bond with both soft tissue and bone.[20] Silicate-based glasses with a wide range of formulations are characterized by a network structure of SiO_4 polyhedra with some orthophosphate (PO_4) substitution.[21] The bioactivity of the glasses depends on the amount of network formers' oxide in glass formulations.[22] The amount of bridging oxygens (BOs) in each SiO_4 tetrahedron determines the bonding environment of network formers, and the overall network connectivity (NC) of the glass. In general, higher bioactivity is associated with a lower NC which favours the release of soluble silica fragments to the solution.[23] To impart a particular property to SiBGs, various amounts of alkali and alkali-earth cations such as CaO and Na_2O can be incorporated in the silicate network.[24] These cations are known as network modifiers that can break some of the Si–O–Si bonds, leading to the formation of non-bridging oxygen atoms (NBOs),[24,25] and depolymerizing the silicate network.[23] The coordination environment, the structural arrangement, and stability of network modifier cations are crucial for the migration mechanism of these ions within the glass structure.[26,27] These key structural factors will subsequently determine the dissolution rate of the SiBGs.[23] The behaviour of different cations and anions was considered in Dietzel's structural model which was an extension to the approach of Zachariasen. Depending on the elements' respective charges, Dietzel was able to define the connection between the size and polarisability of the constituent ions by characterising elements based on Zachariasen's method. He introduced a scheme where the elements in the glass are classified based on their field strength (FS).[28] Based on his definition of field strength, the elements in the glass can be network formers, glass modifiers, or intermediates. He described the field strength as the interacting force between the ionic charge (Z) and the ionic radius between the oxide ions (a)(Z/a^{-2} (Å^{-2})). In his proposed model, the tendency for glass formation increases with increasing field strength.[29]

Copper oxides can be present in glass in both Cu^+ and Cu^{2+} oxidation states during thermal treatments,[30] but Cu^{2+} is the more common oxidation state.[31] However, exactly how Cu incorporates into the BG matrix at the atomic level is still poorly understood. The oxidation state and the introduction of an excessive amount of Cu into BG structures directly impact their performance in terms of bioactivity.[32,33] In addition, the different oxidation states of Cu regulate various biological effects. For instance, Cu^+ ions show considerably more antibacterial effects than Cu^{2+} ions under laboratory conditions.[1,6,34,35] It is also reported that Cu^+ ions show high antimicrobial potency which is achieved at very low surface concentrations of copper ($\sim$5%).[36] Toxicity and killing pathogens by copper-containing materials occur through rapid membrane damage upon the entry of copper ions into cells and degradation of DNA.[37] Both Cu^+ and Cu^{2+} oxidation states play an important role in homeostasis in human cells, but it is Cu^+ that is transported by the major uptake

pathway.[38] It has been found that no adverse effects on glass bioactivity are caused by the incorporation of Cu into the BG network.[39,40] Toxicological effects of Cu-containing BGs on murine cell macrophages have been studied and it was found that it would not cause toxic effects at low concentrations (in the range of up to 0.98 µg mL^{-1} or 2.5 mol%).[41]

Previous studies typically claim that Cu^{2+} ions are responsible species for the antipathogenic effect, and the importance of Cu^+ ions was underestimated.[42–58] Sometimes, the oxidation state of copper is not investigated[44,51] or not investigated with appropriate techniques.

Several analytical techniques can be used to identify the ratio of the oxidation state of different species in solids, including X-ray photoelectron spectroscopy (XPS),[59] electron energy loss spectroscopy (EELS),[60] X-ray absorption spectroscopy (XAS),[61] Raman spectroscopy,[62] and ultraviolet/visible/infrared (UV/vis/IR) spectroscopy.[63] XPS and EELS are perhaps the most widely used tools in materials characterization.[64] The physicochemical properties of the BGs, including the oxidation state of Cu, depend on the selected synthesis method of glasses.[65] Melt-quenching,[66] the sol–gel method,[67] and ion-exchange[39] are effective methods for the production of Cu-containing BGs. It is expected that the two principal oxidation states of Cu exist in the samples synthesized using either the sol–gel method or the melting method, where thermal treatments above 500 °C are applied as reported by Mekki *et al.*[30]

More research must therefore be carried out in order to understand the effective use of Cu-containing BGs, because there are no substantial details about the fundamental underlying mechanism of bioactivity due to the lack of information about their atomistic structure such as the coordination environment, the NBO of *e.g.* network modifier cations and NC of the glasses. The relevant structural information to the glass bioactivity can be well understood and tailored using modern computational techniques such as molecular dynamics (MD) simulations, which in turn unveil other relevant effects.[23,68] MD methods are powerful tools in materials sciences to study amorphous materials and glasses with multiple atomic species,[69] and can be used as a complement to conventional experiments.[70] Besides the experimental effort, the bioactivity of glasses and the degradation rate can be understood using MD simulations.[71] The split network models or NBO and NC can be used to predict the glass bioactivity using MD simulations as effective tools to study glasses. To represent the polarisability of the oxide ions, a shell-model is incorporated into the model.[72] The shell-model is crucial to represent the medium-range structure properly and hence the bioactivity.[73] However, computer modeling of glasses has its own limitations as the time and special scales are largely different between the computer world and the laboratory-based experiments. For example, a much slower cooling rate is needed for the generation of a glass such as 1000 K s^{-1} in the real world, whereas ultrafast cooling rates are used in MD simulation due to the computation time, typically less than a microsecond.[74] Moreover, the new algorithms should be developed to improve computational methods in better representing laboratory glasses.[75]

The method and the condition of glass preparation incorporating Cu ions in the glass structure determines the ratio of $Cu^+:Cu^{2+}$ ions in the glass.[76] In particular, the occurrence of both Cu^+ and Cu^{2+} in the glass depends on a set of temperature, duration and chemical factors in the melt.[77] For example, using CuCl or CuO salts to incorporate Cu ions into the silicate-based glass *via* a melt-quenching method under a nitrogen atmosphere, most ions (around 80–90%) are Cu^+ ions in the glass.[30,78] The ratio of $Cu^{2+}:Cu_{total}$ in Cu-containing phosphate-based glasses was studied by Mugoni *et al.*,[79] and their results were included in the modelling approach by Broglia *et al.*,[80] as we discuss later in the Results section.

We believe that the importance of different oxidation states of Cu in BGs has been underestimated, where the presence of cations in multiple oxidation states can promote different structural changes.[81] The main focus of this paper is to investigate the influence of Cu substitution with both oxidation states in silicate-based glasses at the atomistic scale through the development of a polarisable force field.[72] To the best of our knowledge, this is the first time that the effect of Cu^+ and Cu^{2+} ions simultaneously in the BGs is studied *via* classical MD simulations. We used classical MD to simulate several compositions of copper-containing silicate-based bioactive glasses. Following development and validation of interatomic potentials for Cu^+–O and Cu^{2+}–O, we describe the local environment of the copper atoms, in terms of the pairwise radial distribution function (RDF),[82] coordination number,[23] field strength,[28] network connectivity[83] and bond length. The effect of copper incorporation on the bioactivity of silicate-based glasses is discussed and concluded.

2. Development of interatomic potentials for Cu^+–O and Cu^{2+}–O

Due to the lack of accurate parameters that describe the Cu^+–O and Cu^{2+}–O interactions simultaneously, an accurate interatomic potential was developed to take into account the inclusion of both oxidation states of copper ions in the glass structure. In our classical MD simulations, the interatomic interactions are described by the Born model of solids using full-charge pair potentials. In addition to the electrostatic interactions between ions, the short-range interactions are modelled using the Buckingham potential:

$$U_{ij} = A_{ij}\exp^{\frac{-r_{ij}}{\rho_{ij}}} - C_{ij}r_{ij}^{-6} \tag{1}$$

where r_{ij} is the interatomic distance between two ions i and j and A, ρ, and C are the parameters of the model. The conventional empirical fitting approach was used to obtain the Buckingham potential parameters for the Cu^+–O interaction without contributions from other types of short-range potentials. However, deriving the potential parameters for Cu^{2+}–O interactions was challenging since the interaction in Cu–O shows a strong Jahn–Teller distortion.[84] In 2001, Ermin *et al.* found that the addition of a Morse-type potential can contribute to simple Buckingham and three-body potentials to improve the results

of crystal structure modelling for Cu^{2+}-oxide-containing systems.[85] They claimed that the Buckingham potential, Morse or Lennard-Jones potential cannot describe the Cu^{2+} interactions in crystal structures alone. However, a negative value of the parameter D of the conventional Morse potential (eqn (2)) should be added. This is only a small correction to the Cu^{2+}–O Buckingham potential, but means that the Morse potential parameters cannot be correlated with the real physical quantities of parameter D, or r_0, as is usually done.[85] In the present work, the same method was used and transferability was tested. The Morse potential function is:

$$U_{ij} = D[1 - \exp^{(-b(r_{ij}-r_0))}]^2 - D \tag{2}$$

where conventionally D is the well depth or the bond dissociation energy, r_0 is the equilibrium interatomic distance, and b represents the slope of the potential energy well.

Cu^+–O and Cu^{2+}–O interatomic Buckingham potential parameters were derived using already existing potentials developed for silicate-based glasses. The existing potential parameters are listed in Table 1. The initial crystallographic data were collected from the Inorganic Crystal Structure Data file (ICSD) as a part of the Chemical Data Service at Daresbury.[86] Two crystal structures, $AlCuO_2$ and $KCuO$, were selected to reproduce the potential interaction parameters between Cu^+–O interactions. $Na_2CuSi_3O_8$ and $CaCuO_2$ crystal structures were used for empirical fitting of Cu^{2+}–O interactions.[86] The transferability and reliability of the potentials were improved through a multi-structure empirical fitting.[87,88] The General Utility Lattice Program (GULP) was used for energy minimisation.[89,90] It is crucial to use accurate potentials in order to reproduce experimental data so that the studied structures can be predicted using those potentials when there is no experimental data available. In Table 2 the lattice parameters of the crystalline structures to which the potential was fitted are given. In this system, the accuracy was determined by averaging all unit cell parameters to less than 3% of error between the experimental data and the optimised lattice structure (Table 3). The optimised potential

Table 1 The existing interatomic potential parameters used in this work[85,91,92]

Pairs	Å (eV)	ρ (Å)	C (eV Å^6)
Na–O$_s$	56 465.3453	0.193931	0.0
K–O$_s$	1000.30	0.36198	10.5690
Si–O$_s$	1283.910	0.320520	10.66158
O$_s$–O$_s$	22 764	0.149	27.88
Ca–O$_s$	2152.3566	0.309227	0.09944
P–O$_s$	1020.00	0.343220	0.03

Triplets	(k_{3b}) (eV rad^{-2})	θ (deg)
O$_s$–Si–O$_s$	2.097	109.47
O$_s$–P–O$_s$	3.3588	109.47
O$_s$–Cu^{2+}–O$_s$	4.933	90.0

Core–shell	Core (e)	Shell (e)	k_{cs} (eV Å^{-2})
O$_c$–O$_s$	+0.8482	−2.8482	74.92

Table 2 Optimised potential parameters developed in this work

Pairs	Buckingham		
	Å (eV)	ρ (Å)	C (eV Å^6)
Cu^+–O_s	608.5000	0.275	0.0
Cu^{2+}–O_s	3939.302102	0.285709	0.0

Pair	Morse		
	D (eV)	β (Å^{-1})	r_0 (Å)
Cu^{2+}–O_s	−0.10922	1.359548	3.273

Table 3 The calculated and experimental lattice parameters for copper containing crystals using the interatomic potentials developed in this work

Materials	Parameters	Calc.	Exp.	Diff. (%)
$K_4Cu_4O_4$	a, b	9.505 Å	9.35 Å	1.66
	c	5.524 Å	5.44 Å	1.56
	α, β	90.0°		
	γ	90°		
$AlCuO_2$	a, b	2.867 Å	2.920 Å	1.85
	c	16.981 Å	16.517 Å	−2.73
	α, β	90.0°		
	γ	120°		
$CaCuO_2$	a, b	3.856 Å	3.935 Å	2.06
	c	3.181 Å	3.254 Å	2.31
	α, β, γ	90.0°		
$Na_8Cu_4Si_{12}O_{32}$	a	7.932 Å	7.834 Å	1.24
	b	10.329 Å	10.232 Å	−0.93
	c	9.601 Å	9.783 Å	1.90
	α, γ	90.0°		
	β	105.6°	108.9°	2.31

parameters for Cu^+–O and Cu^{2+}–O interactions were used for the subsequent MD simulations.

3. Simulation details

The DLPOLY code[93] was used to perform classical MD simulations of different copper-containing silicate-based glass compositions. The precise compositions and densities are given in Table 4. In the current study, the compositions were based on the structure of 45S5 BGs with compositions of 46.1 mol% SiO_2, 26.9 mol% CaO, 24.4 mol% Na_2O, and 2.6 mol% P_2O_5 with the Na_2O being gradually substituted by CuO until 20 mol%. The compositions all share the same O/Si ratio, and hence network connectivity. By considering both the oxidation states of Cu, the ratio of $Cu^+ : Cu^{2+}$ was included in the simulation in order to obtain an accurate simulation of the glass structure, as observed experimentally.[30] The percentage of the ratio derived from experimental X-ray photoelectron spectroscopy[30] performed by Mekki *et al.* on silicate-based compositions was used as the starting point to partition the ratio between Cu^+ and Cu^{2+} ions. They reported amounts of Cu^+ = 89% and Cu^{2+} = 10.3% in those glass samples.[30] Since the ratio of $Cu^{2+} : Cu_{total}$ is undetectable for compositions with less than 14 mol% Cu_2O,[30] the composition with 10 mol% of CuO was not simulated in the second batch. The overall charge neutrality of the entire system was maintained by correcting the number of oxygen ions.[80]

Table 4 The glass compositions and densities studied in this work. All compositions are given in mol%

Sample ID	SiO_2	Na_2O	CaO	Cu^+ (mol%)	Cu^{2+}	P_2O_5	Density (g cm^{-3})
$1CuBG_{10}$	46.1	14.4	26.9	10.0	0.00	2.6	3.2069
$1CuBG_{15}$	46.1	9.4	26.9	15.0	0.00	2.6	3.2420
$1CuBG_{20}$	46.1	4.4	26.9	20.0	0.00	2.6	3.2771
$2CuBG_{15}$	46.1	9.4	26.9	13.5	1.5	2.6	3.2420
$2CuBG_{20}$	46.1	4.4	26.9	18.4	1.6	2.6	3.2771

Table 5 The number of atoms studied in this work

Sample ID	O	Si	Na	Ca	Cu^+/Cu^{++}	P
$1.5pt_1CuBG_{10}$	1102	325	188	190	156/0	36
$1CuBG_{15}$	1102	325	132	190	212/0	36
$1CuBG_{20}$	1102	325	62	190	282/0	36
$2CuBG_{15}$	1108	327	134	191	190/11	36
$2CuBG_{20}$	1108	327	62	191	256/14	36

To calculate an accurate ratio of Cu^+ and Cu^{2+} ions in each sample, part of the Cu^+ ions were changed into Cu^{2+} ions manually until an equilibrated system was obtained. In fact, the ratio of Cu^+/Cu^{2+} ions was determined by finding a system in which energy is minimised. Because of this reason, the total ratio of Cu^+ and Cu^{2+} ions varies in each glass composition, depending on the mol% of other ions in the system.

For all these compositions, the initial configuration was set up by placing 2000 atoms independently and randomly into a cubic periodic simulation box with a constant size subject only to the constraint that no two atoms were closer than about 80–90% of their expected interatomic separation. This gives the appropriate density for the compositions and prevents unphysical starting configurations. The densities of the studied compositions were obtained theoretically using a global model for calculating the glass density at room temperature published by Fluegel,[94] and the numbers of atoms are given in Table 5.

Following an instantaneous relaxation at zero temperature, each model was cooled in a series of runs in *NVT* ensembles for 50 ps, decreasing the temperature in the following order at a cooling rate of 4 K ps^{-1}: 2000 K, 1500 K, 1000 K, 650 K, and 300 K, ensuring that the system reached thermal equilibrium for each of the temperatures. The timestep was 0.2 fs, where the cut-offs for short-range potentials and electrostatic interactions were 8 Å and 12 Å, respectively. The Ewald summation method was applied to evaluate the electrostatic force in the system. All data are taken from averages of three independent simulations for each composition. The cooling rates for the classical MD are significantly higher than the ones used in typical experimental rates.[95] This is because a short time scale is used in computer simulation that makes it impossible to simulate the quenching of the system with small cooling rates,[96] but nonetheless the structure is known to be converged even at these cooling rates.[97,98]

4. Results

In the current study, the structures of the Cu-containing silica glasses are characterised, while the comparisons between Cu^+
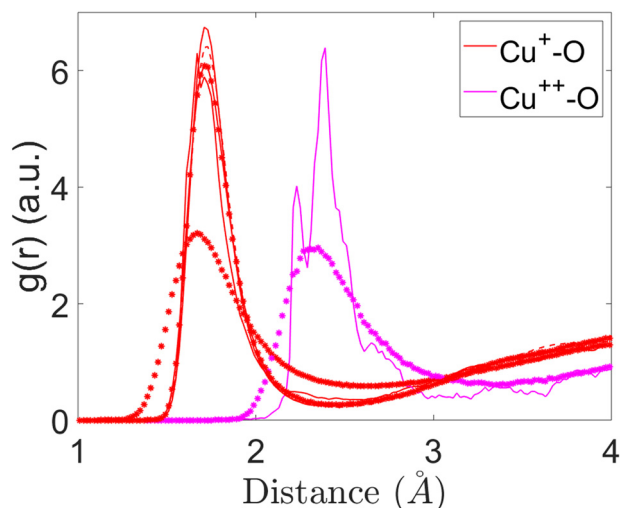
Fig. 1 Partial pair-correlation functions of Cu^+–O and Cu^{2+}–O interactions for the studied compositions.

and Cu^{2+} were carried out to elucidate the differences. The effect of Cu^+ and Cu^{2+} in substitution with Na ions on the structure of 45S5 bioglasses will also be discussed for the first time to the best of our knowledge.

Fig. 1 shows the partial pair-correlation function $g(r)$ as a function of bond length r for Cu^+–O interactions in $1CuSiBG_{10}$, $1CuSiBG_{15}$, and $1CuSiBG_{20}$ compositions. The bond lengths are determined as the first peak of $g(r)$ and coordination numbers are calculated using the information from $g(r)$. As can be seen (Fig. 1), the Cu^+–O bond length is about 1.71 Å for all compositions with just different intensities. The cut-off of 2.1 Å was used to calculate the coordination of Cu^+–O interactions in $1CuSiBG_{15\&20}$. The Cu^+–O interaction exhibits short bond lengths (Fig. 1) in $2CuSiBG_{15}$ and $2CuSiBG_{20}$ compositions, at about 1.68 Å.

Fig. 1 also illustrates the comparison of Cu^{2+}–O interactions between $2CuSiBG_{15}$ and $2CuSiBG_{20}$ compositions. The Cu^{2+}–O average bond distance is longer than that of Cu^+–O in all compositions, but with a different pattern of bonding. The Cu^{2+}–O interaction exhibits a bond length of 2.33 Å and the peak is broader in the $2CuSiBG_{20}$ composition. Whereas, the oxygen neighbours of Cu^{2+} are found at two different distances of 2.33 Å and 2.39 Å in the composition with a lower concentration of Cu (15 mol%). Table 6 presents the mean of bond length and coordination numbers for each Cu oxide.

Table 7 Short-intermediate range structures for Cu^{2+} ions in the studied compositions

Sample ID	Si–O···Cu^{2+} (Å)	P–O···Cu^{2+} (Å)
$2CuSiBG_{15}$	3.73 ± 0.14	3.19 ± 0.19
$2CuSiBG_{20}$	3.53 ± 0.14	3.47 ± 0.19

We identified another short-intermediate range structure in the glass due to the presence of Cu^{2+} ions which promotes the binding of Cu^{2+} ions to the glass network formers by relatively covalent bonds. This may produce P–O···Cu^{2+} or Si–O···Cu^{2+} bonds.[80] We computed this for Cu^{2+} ions present in the studied compositions here. The results are presented in Table 7. From the results it can be seen that Si–O···Cu and P–O···Cu distances are approximately 3.19–3.73 Å.

4.1. Cation coordination numbers

The coordination numbers of both Cu^+ and Cu^{2+} cations were analysed and presented in Table 6. It was found that the CNs of Cu^+ and Cu^{2+} ions change as a function of the oxidation state. The average CNs of Cu^+–O and Cu^{2+}–O were calculated to be 3.04 ± 0.27 and 6.05 ± 0.07, respectively. The CNs in Cu^+ are lower than those in Cu^{2+} ions with a higher oxidation state, which has profound effects on bioactivity. The bond length also increases as the CN increases for the Cu^{2+} ions. As can be seen, the Cu^+–O and Cu^{2+}–O CNs do not differ drastically with the changing composition.

Typical oxygen arrangements around Cu^+ are shown in Fig. 2. Cu^+ ions could be found coordinated by two and three oxygen atoms in the arrangement of linear and trigonal geometries, respectively. In all studied compositions, the geometry of Cu^+–O is mainly trigonal with three oxygen atoms at a distance of about 1.68–1.71 Å. The coordination environment of Cu^{2+} ions are shown in molecular geometries as shown in Fig. 3 and as can be seen Cu^{2+} ions are surrounded by six oxygen atoms. The results show a complex with regular octahedral geometries (Fig. 3(a)) where the oxygen atoms are at the same distance from the Cu^{2+} central atom. A distorted octahedral geometry (Fig. 3(b)) has been observed for Cu^{2+} in composition with a lower Cu concentration where the oxygen atoms are surrounding the central atoms at two different distances based on the results from the pair-correlation function.
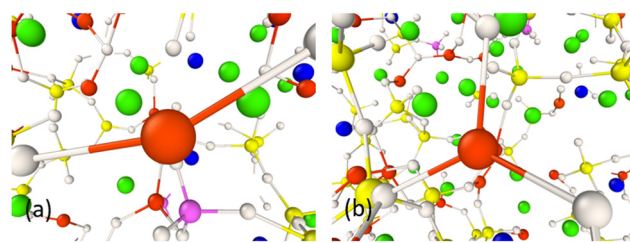
Table 6 The Cu–O bond-lengths (Å) and coordination numbers of the Cu^{2+}–O interactions studied

Sample ID	Oxide	Bond length (Å)	CN		
			Total	BO	NBO
$1CuSiBG_{10}$	Cu^+	1.71	3.0	0.2	2.8
$1CuSiBG_{15}$	Cu^+	1.71	2.9	0.1	2.8
$1CuSiBG_{20}$	Cu^+	1.71	2.8	0.1	2.7
$2CuSiBG_{15}$	Cu^+	1.67	3.0	0.1	2.9
$2CuSiBG_{20}$	Cu^+	1.69	3.0	0.4	2.6
$2CuSiBG_{15}$	Cu^{2+}	2.23–2.39	6.1	1.6	4.5
$2CuSiBG_{20}$	Cu^{2+}	2.31	6.0	0.8	5.2

Fig. 2 Snapshot of (a) linear and (b) trigonal structures of Cu^+ ions in 1CuSiBG compositions. The colours are P (magneta), O (white), Ca (green), Na (navy), and Cu (red).
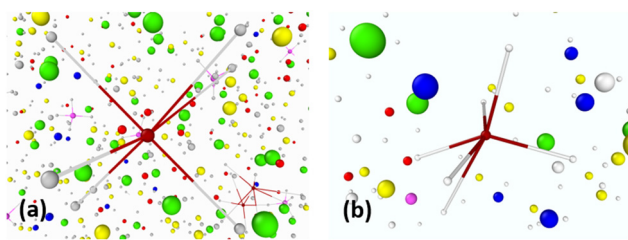
Fig. 3 Snapshot of (a) regular octahedral and (b) distorted octahedral structures of Cu^{2+} in 1CuSiBG$_{20}$ and 2CuSiBG$_{15}$ compositions, respectively. The images were obtained by OVITO. The colours are P (magenta), O (white), Ca (green), Na (navy), Cu^+ (red) and Cu^{2+} (dark red).

4.2. Distribution of NBO

The percentage of NBO atoms in the first coordination shell of the cations in the studied compositions is shown in Fig. 4 and 5. This shows that in 1CuSiBGs$_{10,15,20}$ compositions Cu^+ has more NBO in its first coordination shell than Ca and Na ions. Also the percentage of NBO increases with an increase in the mol% of Cu_2O in the glass as substituted with Na_2O. The percentage of NBO provided by Ca is approximately similar in all compositions, and that for Na decreases. Table 8 shows the calculated field strength[28] of cations based on their bond lengths in the 2CuSiBGs$_{20}$ composition where both Cu^+ and Cu^{2+} ions are present. From Table 8, Na has the smallest field strength (0.18) and Ca and Cu^{2+} show similar field strengths. It can be seen in Fig. 5, where the percentage distributions of NBO in the first coordination shell of Cu^2 and Ca are about 85% which can explain the similarity of the these two ions' field strength. Thus, the three Ca, Na, and Cu^+ cations fall into network modifier classes. From Fig. 5, increasing the mol% of Cu_2O during substitution with Na_2O decreases the percentage of NBO provided by Cu^+ ions in the 2CuSiBG$_{20}$ composition.

The bioactivity of the implemented glasses is controlled by the network connectivity of the glass as the key parameter.[99] The network connectivity is defined as the average number of BO atoms per silicon atom.[91] As can be seen from Fig. 4 and 5, the NBO atoms provided by Si–O interactions are similar in all studied compositions. It seems the substitution of Na for Cu^+ and Cu^{2+} does not change the network connectivity, nor would
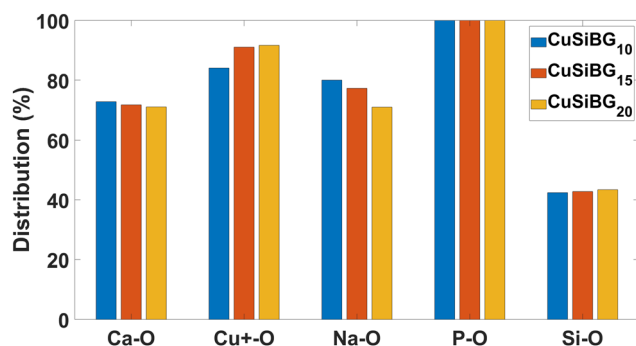

Fig. 4 The percentage of NBO in the first coordination shell of all atoms in 1CuSiBGs$_{10}$ 1CuSiBGs$_{15}$, and 1CuSiBGs$_{20}$ compositions.
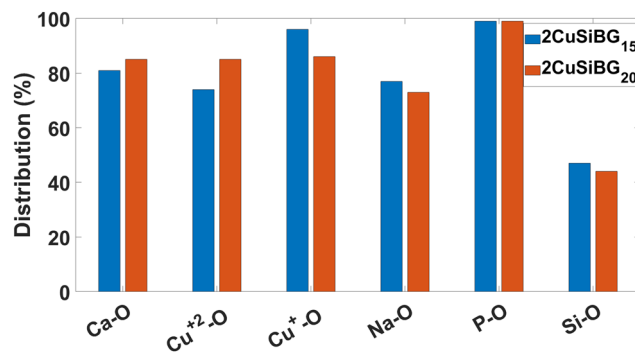

Fig. 5 The percentage of NBO in the first coordination shell of all atoms in 2CuSiBGs$_{15}$ and 2CuSiBGs$_{20}$ compositions.

Table 8 Calculated field strengths of cations in the 2CuSiBGs$_{20}$ composition

Ion	Interatomic distance (Å)	Field strength (Z/a^2) (e Å^{-2})
Na^+	2.34	0.18
Cu^+	1.69	0.35
Cu^{2+}	2.33	0.36
Ca^{2+}	2.33	0.36
Si^{4+}	1.61	1.54
P^{5+}	1.53	2.13

we expect this, as the O/Si ratio is constant across all of our studied compositions.

5. Discussion

The present paper focusses on Cu-containing silicate-based glasses for use in tissue engineering. Previously, the addition of Cu^+ ions into the basic BG composition has been only studied experimentally to investigate their effect on biological tissues.[100] To the best of our knowledge, this is the first time that the effect of Cu^+ and Cu^{2+} ions simultaneously in BGs is studied *via* classical MD simulations. The aim of the project is to describe precisely the effect of Cu ions in the structure of silicate-based BGs to understand the effects on the bioactivity. Based on the published studies, the Cu ions can occur in the glass in both Cu^+ and Cu^{2+} oxidation states using conventional melting methods.[30]

It was found by our study that Cu^+ ions can be linear two-coordinated geometry and/or trigonal coordinated geometry within silicate-based BG (Fig. 2). Our findings show excellent agreement with the study conducted recently by Galante *et al.*,[101] The Cu^+–O bond shows a complicated bonding nature with both ionic and covalent characteristics.[102] The charge transfer takes place from the Cu 4s shell to the 2p shell of O. The Cu 3d shells also interact with the 2p shell of O, but the net contribution is negligible. This is because the bonding and anti-bonding components cancel each other.[103] The interaction between Cu and O was found to be predominantly covalent and the intermolecular O–O interaction is dominated by Coulomb repulsion. A linear structure can also be formed and this is due

to the strong hybridisation of the O 2p shell with Cu 3d, forming bonding and anti-bonding linear combinations.[104] From the results, it is clearly observable that linear coordinated Cu^+ can be found in the system that contains a higher [Cu^+/Cu_{total}] ratio, as we observe.

Our results (Fig. 3) show that Cu^{2+} exhibits octahedral geometries surrounded by six oxygen ions. Fig. 6 illustrates two prototypical Jahn–Teller distortions of an octahedral Cu^{2+} complex, compressed and elongated. The two distorted octahedral complexes are theoretically possible, but in practice elongated complexes are more common by far[84] and no study has reported Jahn–Teller compressions for Cu^{2+}. Also no noticeable linear structure can be seen in both 2Cu20SiBG and 2Cu15SiBG systems, where both Cu^+ and Cu^{2+} were included. The electron distribution and the arrangement of atoms within the Cu^{2+} complexes are strongly affected by Jahn–Teller distortions.

The ratio between the ions is dependent on the glass composition. From the results, the coordination environment for Cu^+ is predominantly 3 and that for Cu^{2+} is 6. In 1992, Kamiya et al. studied copper-containing alumino-silicate based glasses with a CuO concentration of 20 wt% and reported a coordination number of 2 for Cu^+ and 4 for Cu^{2+}.[76] Later on in 2012, Silvestri et al. conducted a similar study using the X-ray Absoption Spectroscopy (XAS) technique and confirmed the results in Kamiya's study.[105] Another study was performed recently in 2019 by Grund et al.[106] to investigate the Cu^+ and Cu^{2+} coordination environments in mixed alkali-lime-silicate glasses using X-ray and UV-Vis-NIR absorption spectroscopy. It was concluded that Cu^+ is coordinated by two oxygen ions, whereas Cu^{2+} has a coordination of six oxygen ions.[76,105,106] However, according to Grund et al., it is unlikely that all Cu^+ ions are coordinated in a linear way with oxygen ions in amorphous materials such as glasses. Therefore, it is likely that Cu^+–O coordination with a coordination number of three, as we observed, also occurs, which was neglected in these studies. The findings from our study using the MD method proves that Cu^+ can be coordinated by two and three oxygen ions within the glass systems.

For both Cu^+ and Cu^{2+}, previous experiments have reported a broad range of bond lengths, with which our results are consistent. Previous studies reported a distance of 1.79–2.32 Å for Cu^+–O in crystalline Cu_2O.[101,105,107–112] It was found that the distance between Cu^+–O interactions is slightly shorter in crystalline systems than in glassy systems. In the present study,

it was found that the Cu^+–O interaction with a distance in the range of 1.68–1.71 Å is slightly shorter than all the mentioned investigations of Cu in glass. Three oxygen atoms at 1.71 Å gives rise to trigonally coordinated Cu^+ atoms in $1CuSiBG_{10,15,20}$ compositions, whereas the primary shorter Cu^+–O bond length is associated with a similar coordination in $2CuSiBG_{15,20}$ compositions. Cu^{2+} atoms were found to be coordinated by six oxygen atoms in an octahedral environment with the distance ranging between 2.23 Å and 2.39 Å. When an octahedral complex is distorted towards an elongated octahedron, two longer axial bonds and four equatorial shorter bonds are expected in the complex.[84] The two axial Cu^{2+}–O interactions of 2.1–2.9 Å have been reported as the most common bond length.[113] A bond length of 2.4 Å has also been reported for axial interactions.[84] The axial interaction in the range of 2.4–2.9 Å is considered as weaker, secondary, and predominantly electrostatic in nature.[84] In addition, any interaction longer than 2.8 Å is considered as a van der Waals interaction only.[84] In 2019, another study reported a bond length in the range of 1.89–1.91 Å for the equatorial Cu^{2+}–O interactions in the glass compositions.[106] In the same study the bond distances ranging from 2.20 to 2.24 Å have been reported for the Cu^{2+}–O axial interactions. In the present study a sharp peak around 2.32 Å for Cu^{2+}–O interactions in the 2Cu15SiBG composition can be associated with an axial bond length. Thus, in silicate-based BGs, Cu^{2+}–O distances are shorter than those interactions in crystalline systems. However, it was also shown by the Mössbauer spectroscopy method that the coordination number and bond length of copper ions in silicate-based glasses depends on the composition.[114]

From the results presented in Fig. 4 and 5, it can be seen that the amount of Si-NBO bonding in the glass structure is within the range from 42 to 44% in all compositions. From this, it is assumed that the glass network connectivity remains unchanged by adding Cu^+ and Cu^{2+} ions into the glass. The polarizability, mobility due to charges on ions, field strength, and concentration of ions within the BG structures are the key factors in determining the location and distribution of cations in the glass network. The size of ions are less important when the ions are replaced with the ones with similar ionic radii. However, the charge differences between the cations determine their distributions in the glass structure.[115]

When a melt of Cu^{2+} salt is used for implanting Cu into the glass, the Cu^{2+} ions initially are predominantly incorporated into glass. Then, the ions are reduced partially into their Cu^+ state due to the singly charged vacancies of alkali ions in the glass network.[116] It is likely that by increasing the concentration of divalent Cu salt, fewer Cu^{2+} ions will tend to be located near lone electron pairs of NBO atoms. From our results, the Cu^{2+} ions are assumed to form four short ionic bonds and two long polarized covalent bonds. In this case, the equatorial Cu^{2+}–O bond length turns out to be similar to that of Cu^+–O (2.23 Å).[106] Based on the results (Table 6) for the 2Cu15SiBG composition, about two (1.6) of the six oxygen atoms around Cu^{2+} can be BO and the rest form NBO. Cu^{2+} ions with a higher charge than Cu^+ in the glass network
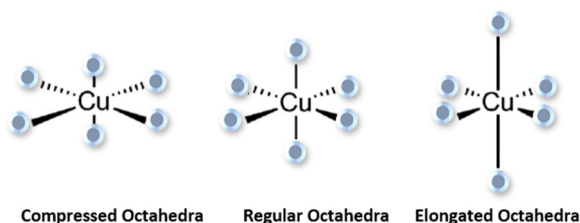

Fig. 6 Schematic presentation of compressed and elongated octahedral Cu^{2+} complexes.

promoted the formation of a short-intermediate range structure (Table 7) and produced relatively covalent P–O–Cu^{2+} bonds, leading to more BO arrangements in the glass.[117] It also causes a reduction of optimum sites for Cu^+, reducing the number of NBO for this ion.

Our study indicates that Cu^+ and Cu^{2+} bond-lengths and coordination numbers vary in different glass systems. However, the bioactivity of silicate-based glasses in terms of Si-NBO bonding in the glass network will remain unchanged following the inclusion of Cu in its both form of oxidation states, Cu^+ and Cu^{2+}. Apart from the network connectivity of the glass, the field strength of modifier cations can also influence on the bioactivity and dissolution behaviour of the glass.[118] For example, Ca and Na ions have different effects on physical and chemical durability due to having different field strengths and bonding to the network structure. Calcium ions with higher field strength can bond to the glass network and increase the mechanical strength and durability of silicate-based glasses.[118] It was found in the present study that Ca and Cu^+ as well as Cu^{2+} show a similar field strength and the NBO percentage distribution decreases upon increasing the Cu^{2+} ions in the glass. We would not expect substantial changes in the bioactivity after the incorporation of copper, regardless of the oxidation state. A study conducted by Bejarano *et al.* also evidenced experimentally that by incorporating Cu^{2+} ions with substitution by CaO, the glass dissolution and the ion release became more difficult and due to a more stabilized glass structure.[119] The fundamental mechanism behind this can be explained from our results. However, they have also not mentioned the presence of Cu^+ ions in the glass due to the lack of information about the atomistic structure of Cu-incorporated BGs. When there is more than one modifier in the glass system, they compete for NBO with higher field strength cations within them.[120]

6. Conclusions

We have conducted classical molecular dynamics simulations of various copper-containing silicate glasses to characterize the Cu^+ and Cu^{2+} ions' local environment within the bioactive silicate-based glasses and to understand the influence of both oxides on the structure and bioactivity of the glasses. Optimised potential parameters of Cu^+–O and Cu^{2+}–O interactions were developed and applied for subsequent molecular dynamics simulations.

It was found that the structural effect of the addition of Cu^{2+} ions to silicate-based glasses can be investigated using MD models in the presence of Cu^+ ions simultaneously in a certain ratio. We have found that the Cu^+–O bond length with a planar geometry and coordination number of three is shorter than the Cu^{2+}–O interactions' elongated octahedral geometry. The incorporated copper oxides in the structure of silicate-based glasses are expected to act as network modifiers. However, some Cu^{2+} ions bond to non-bridging oxygen atoms. The effect on the bioactivity of Cu incorporation is likely to be small.

Data availability

Data for this paper, including input files for DLPOLY, and analysis codes used to generate the results from the output, are available at **https://doi.org/10.17028/rd.lboro.22294123.v1**.

Conflicts of interest

There are no conflicts to declare.

Acknowledgements

References

1 G. Borkow, *Curr. Chem. Biol.*, 2015, **8**, 89–102.

2 M. Bost, S. Houdart, M. Oberli, E. Kalonji, J.-F. Huneau and I. Margaritis, *J. Trace Elem. Med. Biol.*, 2016, **35**, 107–115.

3 G. Lockitch, A. C. Halstead, L. Wadsworth, G. Quigley, L. Reston and B. Jacobson, *Clin. Chem.*, 1988, **34**, 1625–1628.

4 R. S. Gibson, *Principles of nutritional assessment*, Oxford University Press, Oxford, 2005.

5 M. Angelova, S. Asenova, V. Nedkova and R. Koleva-Kolarova, *Trakia J. Sci.*, 2011, **9**, 88–98.

6 M. Solioz, *Mycobact. Dis.*, 2016, **6**(2), 1–4.

7 H. Tapiero, D. M. Townsend and K. D. Tew, *Biomed. Pharmacother.*, 2003, **57**, 386–398.

8 J. Osredkar, *J. Clin. Toxicol.*, 2011, S:3, DOI: **10.4172/2161-0495.s3-001**.

9 G. Borkow and J. Gabbay, *Curr. Chem. Biol.*, 2009, **3**, 272–278.

10 C. Li, Y. Li and C. Ding, *Int. J. Mol. Sci.*, 2019, **20**, 175.

11 R. Uauy, M. Olivares and M. Gonzalez, *Am. J. Clin. Nutr.*, 1998, **67**, 952S959S.

12 W. Feng, F. Ye, W. Xue, Z. Zhou and Y. J. Kang, *Mol. Pharmacol.*, 2008, **75**, 174–182.

13 S. Kargozar, M. Mozafari, S. Ghodrat, E. Fiume and F. Baino, *Mater. Sci. Eng., C*, 2020, 111741.

14 A. P. Ingle, N. Duran and M. Rai, *Appl. Microbiol. Biotechnol.*, 2013, **98**, 1001–1009.

15 F. Baino, I. Potestio and C. Vitale-Brovarone, *Materials*, 2018, **11**, 1524.

16 S. Kargozar, S. Hamzehlou and F. Baino, *Materials*, 2017, **10**, 1429.

17 F. Baino, S. Hamzehlou and S. Kargozar, *J. Funct. Biomater.*, 2018, **9**, 25.

18 M. Fábián, Z. Kovács, J. L. Lábár, A. Sulyok, Z. E. Horváth, I. Székács and V. Kovács Kis, *J. Mater. Sci.*, 2019, **55**, 2303–2320.

19 J. R. Jones, *Acta Biomater.*, 2013, **9**, 4457–4486.

20 N. Al-Harbi, H. Mohammed, Y. Al-Hadeethi, A. S. Bakry, A. Umar, M. A. Hussein, M. A. Abbassy, K. G. Vaidya, G. Al Berakdar, E. M. Mkawi and M. Nune, *Pharmaceuticals*, 2021, **14**, 75.

21 I. Elgayar, A. E. Aliev, A. R. Boccaccini and R. G. Hill, *J. Non-Cryst. Solids*, 2005, **351**, 173–183.

22 S. Kaya, M. Cresswell and A. R. Boccaccini, *Mater. Sci. Eng., C*, 2018, **83**, 99–107.

23 A. Tilocca, *Phys. Rev. B*, 2007, **76**, 224202.

24 J. Sułowska, I. Wacławska and M. Szumera, *J. Therm. Anal. Calorim.*, 2012, **109**, 705–710.

25 H. Scholze, *Glass nature, structure, and properties*, New York Berlin Heidelberg London Paris Tokyo Hong Kong Barcelona Springer, 1991.

26 C. Karlsson, E. Zanghellini, J. Swenson, B. Roling, D. T. Bowron and L. Börjesson, *Phys. Rev. B*, 2005, **72**, 064206.

27 H. Lammert and A. Heuer, *Phys. Rev. B*, 2004, **70**, 024204.

28 S. J. Watts, R. G. Hill, M. D. ODonnell and R. V. Law, *J. Non-Cryst. Solids*, 2010, **356**, 517–524.

29 K. Stanton, PhD thesis, University of Limerick, 2000.

30 A. Mekki, D. Holland and C. F. McConville, *J. Non-Cryst. Solids*, 1997, **215**, 271–282.

31 W. Grochala and Z. Mazej, *Philos. Trans. R. Soc., A*, 2015, **373**, 20140179.

32 E. Metwalli, *J. Non-Cryst. Solids*, 2003, **317**, 221–230.

33 J. Sułowska, I. Wacławska and M. Szumera, *J. Therm. Anal. Calorim.*, 2012, **109**, 705–710.

34 S. Mathews, R. Kumar and M. Solioz, *Appl. Environ. Microbiol.*, 2015, **81**, 6399–6403.

35 M. Hans, A. Erbe, S. Mathews, Y. Chen, M. Solioz and F. Mücklich, *Langmuir*, 2013, **29**, 16160–16166.

36 T. M. Gross, J. Lahiri, A. Golas, J. Luo, F. Verrier, J. L. Kurzejewski, D. E. Baker, J. Wang, P. F. Novak and M. J. Snyder, *Nat. Commun.*, 2019, **10**, 1979.

37 C. E. Santo, E. W. Lam, C. G. Elowsky, D. Quaranta, D. W. Domaille, C. J. Chang and G. Grass, *Appl. Environ. Microbiol.*, 2010, **77**, 794–802.

38 J. H. Kaplan and E. B. Maryon, *Biophys. J.*, 2016, **110**, 7–13.

39 M. Miola and E. Verné, *Materials*, 2016, **9**, 405.

40 M. Mozafari, S. Banijamali, F. Baino, S. Kargozar and R. G. Hill, *Acta Biomater.*, 2019, **91**, 35–47.

41 G. Kaur, N. Sriranganathan, S. G. Waldrop, P. Sharma and B. N. Chudasama, *Biomed. Mater.*, 2017, **12**, 045020.

42 E. A. Abou Neel, I. Ahmed, J. Pratten, S. N. Nazhat and J. C. Knowles, *Biomaterials*, 2005, **26**, 2247–2254; A. Bonici, G. Lusvardi, G. Malavasi, L. Menabue and A. Piva, *J. Eur. Ceram. Soc.*, 2012, **32**, 2777–2783.

43 V. Aina, G. Cerrato, G. Martra, G. Malavasi, G. Lusvardi and L. Menabue, *Appl. Surf. Sci.*, 2013, **283**, 240–248.

44 E. Wers and L. Bunetel, *Bioceram. Dev. Appl.*, 2013, S:1, DOI: 10.4172/2090-5025.s1-013.

45 C. Wu, Y. Zhou, M. Xu, P. Han, L. Chen, J. Chang and Y. Xiao, *Biomaterials*, 2013, **34**, 422–433.

46 H. Palza, B. Escobar, J. Bejarano, D. Bravo, M. Diaz-Dosque and J. Perez, *Mater. Sci. Eng., C*, 2013, **33**, 3795–3801.

47 J. Bejarano, P. Caviedes and H. Palza, *Biomed. Mater.*, 2015, **10**, 025001.

48 Y. Lin, W. Xiao, B. S. Bal and M. N. Rahaman, *Mater. Sci. Eng., C*, 2016, **67**, 440–452.

49 H. Wang, S. Zhao, W. Xiao, J. Xue, Y. Shen, J. Zhou, W. Huang, M. N. Rahaman, C. Zhang and D. Wang, *Mater. Sci. Eng., C*, 2016, **58**, 194–203.

50 A. Bari, N. Bloise, S. Fiorilli, G. Novajra, M. Vallet-Regí, G. Bruni, A. Torres-Pardo, J. M. González-Calbet, L. Visai and C. Vitale-Brovarone, *Acta Biomater.*, 2017, **55**, 493–504; K. Zheng, X. Dai, M. Lu, N. Hüser, N. Taccardi and A. R. Boccaccini, *Colloids Surf., B*, 2017, **150**, 159–167.

51 R. Koohkan, T. Hooshmand, D. Mohebbi-Kalhori, M. Tahriri and M. T. Marefati, *ACS Biomater. Sci. Eng.*, 2018, **4**, 1797–1811.

52 M. Miola, A. Cochis, A. Kumar, C. Arciola, L. Rimondini and E. Verné, *Materials*, 2018, **11**, 961.

53 B. A. E. Ben-Arfa, S. Neto, M. Salvado, R. C. Pullar and J. M. F. Ferreira, *Acta Biomater.*, 2019, **87**, 1742–7061.

54 S. Mokhtari and A. W. Wren, *Biomed. Glasses*, 2019, **5**, 13–33.

55 S. Kapoor, D. Brazete, I. C. Pereira, G. Bhatia, M. Kaur, L. F. Santos, D. Banerjee, A. Goel and J. M. F. Ferreira, *J. Non-Cryst. Solids*, 2019, **506**, 98–108.

56 R. Lin, C. Deng, X. Li, Y. Liu, M. Zhang, C. Qin, Q. Yao, L. Wang and C. Wu, *Theranostics*, 2019, **9**, 6300–6313.

57 S. Akhtach, Z. Tabia, K. El Mabrouk, M. Bricha and R. Belkhou, *Ceram. Int.*, 2021, **47**, 424–433.

58 J. Jiménez-Holguín, S. Sánchez-Salcedo, M. Vallet-Regí and A. J. Salinas, *Microporous Mesoporous Mater.*, 2020, **308**, 110454.

59 F. Zhang, P. Wang, J. Koberstein, S. Khalid and S.-W. Chan, *Surf. Sci.*, 2004, **563**, 74–82.

60 L. A. J. Garvie and P. R. Buseck, *J. Phys. Chem. Solids*, 1999, **60**, 1943–1947.

61 A. M. Shahin, F. Grandjean, G. J. Long and T. P. Schuman, *Chem. Mater.*, 2004, **17**, 315–321.

62 T. Taniguchi, T. Watanabe, N. Sugiyama, A. K. Subramani, H. Wagata, N. Matsushita and M. Yoshimura, *J. Phys. Chem. C*, 2009, **113**, 19789–19793.

63 A. S. Karakoti, S. Singh, A. Kumar, M. Malinska, S. V. N. T. Kuchibhatla, K. Wozniak, W. T. Self and S. Seal, *J. Am. Chem. Soc.*, 2009, **131**, 14144–14145.

64 C. M. Sims, R. A. Maier, A. C. Johnston-Peck, J. M. Gorham, V. A. Hackley and B. C. Nelson, *Nanotechnology*, 2018, **30**, 085703.

65 S. Kargozar, S. Ramakrishna and M. Mozafari, *Curr. Opin. Biomed. Eng.*, 2019, **10**, 181–190.

66 S. Kapoor, D. Brazete, I. C. Pereira, G. Bhatia, M. Kaur, L. F. Santos, D. Banerjee, A. Goel and J. M. F. Ferreira, *J. Non-Cryst. Solids*, 2019, **506**, 98–108.

67 R. Koohkan, T. Hooshmand, M. Tahriri and D. Mohebbi-Kalhori, *Ceram. Int.*, 2018, **44**, 2390–2399.

68 J. Du and L. R. Corrales, *Phys. Rev. B*, 2005, **72**, 092201.

69 M. Montazerian, E. D. Zanotto and J. C. Mauro, *Int. Mater. Rev.*, 2019, **65**, 297–321.

70 J. Meller, *Molecular Dynamics*, John Wiley & Sons., 2001.

71 R. G. Hill and D. S. Brauer, *J. Non-Cryst. Solids*, 2011, **357**(24), 3884–3887.

72 B. G. Dick and A. W. Overhauser, *Phys. Rev.*, 1958, **112**, 90–103.

73 A. Tilocca, *J. Chem. Phys.*, 2008, **129**, 084504.

74 J. Ding, Y. Q. Cheng and E. Ma, *Acta Mater.*, 2014, **69**, 343–354.

75 J. Ding and E. Ma, *npj Comput. Mater.*, 2017, **3**(9), 1–12.

76 K. Kamiya, T. Yoko and S. Sakka, *J. Non-Cryst. Solids*, 1986, **80**, 405–411.

77 F. Gonella, A. Quaranta, S. Padovani, C. Sada, F. DAcapito, C. Maurizio, G. Battaglin and E. Cattaruzza, *Appl. Phys. A: Mater. Sci. Process.*, 2005, **81**, 1065–1071.

78 S. Sakka, K. Kamiya and K. Kato, *J. Non-Cryst. Solids*, 1982, **52**, 77–90.

79 C. Mugoni, H. Jain, M. Montorsi, M. Montecchi, A. Kovalskiy and C. Siligardi, *J. Non-Cryst. Solids*, 2016, **447**, 91–97.

80 G. Broglia, C. Mugoni, J. Du, C. Siligardi and M. Montorsi, *J. Non-Cryst. Solids*, 2014, **403**, 53–61.

81 D. W. Davies, K. T. Butler, O. Isayev and A. Walsh, *Faraday Discuss.*, 2018, **211**, 553–568.

82 Democritus: The Radial Distribution Function, **https://people.bath.ac.uk/chsscp/teach/md.bho/Theory/rdf.html**, (accessed 4 August 2022).

83 G. Kaur, *Clinical applications of biomaterials: state-of-the-art progress, trends, and novel approaches*, Springer, Cham, Switzerland, 2017.

84 M. A. Halcrow, *Chem. Soc. Rev.*, 2013, **42**, 1784–1795.

85 N. N. Eremin, L. I. Leonyuk and V. S. Urusov, *J. Solid State Chem.*, 2001, **158**, 162–168.

86 D. A. Fletcher, R. F. McMeeking and D. Parkin, *J. Chem. Inf. Comput. Sci.*, 1996, **36**, 746–749.

87 C. Randall, *Rev. Mineral. Geochem.*, 2001, **42**, 1–35.

88 P. Tiwary, A. van de Walle and N. Grønbech-Jensen, *Phys. Rev. B*, 2009, **80**, 174302.

89 S. T. Bromley, S. A. French, A. A. Sokol, C. R. A. Catlow and P. Sherwood, *J. Phys. Chem. B*, 2003, **107**, 7045–7057.

90 L. Yang, A. Karim and J. T. Muckerman, *J. Phys. Chem. C*, 2013, **117**, 3414–3425.

91 J. K. Christie and N. H. de Leeuw, *J. Mater. Sci.*, 2017, **52**, 9014–9022.

92 P. Smok, *J. Phys.: Conf. Ser.*, 2011, **289**, 012030.

93 W. Smith and T. R. Forester, *J. Mol. Graphics*, 1996, **14**, 136–141.

94 A. Fluegel, *J. Am. Ceram. Soc.*, 2007, **90**, 2622–2625.

95 A. Tilocca, A. N. Cormack and N. H. de Leeuw, *Chem. Mater.*, 2006, **19**, 95–103.

96 K. Vollmayr, W. Kob and K. Binder, *Phys. Rev. B: Condens. Matter Mater. Phys.*, 1996, **54**, 15808–15827.

97 A. Tilocca, *Proc. R. Soc. A*, 2009, **465**, 1003–1027.

98 K. Vollmayr-Lee, W. Kob, K. Binder and A. Zippelius, *Int. J. Mod. Phys. C*, 1999, **10**, 1443–1451.

99 R. Hill, *J. Mater. Sci. Lett.*, 1996, **15**, 1122–1125.

100 S. N. Rath, A. Brandl, D. Hiller, A. Hoppe, U. Gbureck, R. E. Horch, A. R. Boccaccini and U. Kneser, *PLoS One*, 2014, **9**, e113319.

101 M. Tayar Galante, A. Živković, J. C. Alvim, C. C. Calchi Kleiner, M. Sangali, S. F. R. Taylor, A. J. Greer, C. Hardacre, K. Rajeshwar, R. Caram, R. Bertazzoli, R. T. Macaluso, N. H. de Leeuw and C. Longo, *ACS Appl. Mater. Interfaces*, 2021, **13**, 32865–32875.

102 L. Wang, H. Wu, S. R. Desai and L. Lou, *Phys. Rev. B: Condens. Matter Mater. Phys.*, 1996, **53**(12), 8028–8031.

103 M. Jansen and J. C. Schon, *Structure Prediction in Solid-State Chemistry as an Approach to Rational Synthesis Planning*, Elsevier Ltd, 2013.

104 C. Gattinoni and A. Michaelides, *Surf. Sci. Rep.*, 2015, **70**, 424–447.

105 A. Silvestri, S. Tonietto, F. DAcapito and G. Molin, *J. Cult. Herit.*, 2012, **13**, 137–144.

106 L. Grund Bäck, S. Ali, S. Karlsson, L. Wondraczek and B. Jonson, *J. Non-Cryst. Solids: X*, 2019, **3**, 100029.

107 F. DAcapito, S. Colonna, S. Mobilio, F. Gonella, E. Cattaruzza and P. Mazzoldi, *Appl. Phys. Lett.*, 1997, **71**, 2611–2613.

108 F. DAcapito, S. Mobilio, J. R. Regnard, E. Cattaruzza, F. Gonella and P. Mazzoldi, *J. Non-Cryst. Solids*, 1998, **232–234**, 364–369.

109 K. Fukumi, A. Chayahara, K. Kadono, H. Kageyama, T. Akai, N. Kitamura, M. Makihara, K. Fujii and J. Hayakawa, *J. Non-Cryst. Solids*, 1998, **238**, 143–151.

110 J. Lee, T. Yano, S. Shibata, A. Nukui and M. Yamane, *J. Non-Cryst. Solids*, 2000, **277**, 155–161.

111 C. Maurizio, F. dAcapito, M. Benfatto, S. Mobilio, E. Cattaruzza and F. Gonella, *Eur. Phys. J. B*, 2000, **14**, 211–216.

112 L. Tröger, T. Yokoyama, D. Arvanitis, T. Lederer, M. Tischer and K. Baberschke, *Phys. Rev. B: Condens. Matter Mater. Phys.*, 1994, **49**, 888–903.

113 B. Murphy, *Coord. Chem. Rev.*, 2003, **243**, 237–262.

114 F. dAcapito, S. Mobilio, G. Battaglin, E. Cattaruzza, F. Gonella, F. Caccavale, P. Mazzoldi and J. R. Regnard, *J. Appl. Phys.*, 2000, **87**, 1819–1824.

115 I. A. Demichev, A. I. Sidorov, N. V. Nikonorov and T. A. Shahverdov, *Sci. Tech. J. Inf. Technol., Mech. Opt.*, 2015, 54–59.

116 I. Demichev, N. Nikonrov and A. Sidorov, *Ion Exch.: Theory Appl.*, 2017, 251–312.

117 M. Suszynska, M. Maczka, M. Ptak and L. Krajczyk, *J. Non-Cryst. Solids*, 2014, **401**, 92–95.

118 Y. Xiang and J. Du, *Chem. Mater.*, 2011, **23**, 2703–2717.

119 J. Bejarano, P. Caviedes and H. Palza, *Biomed. Mater.*, 2015, **10**, 025001.

120 S. Watts, PhD thesis, Imperial College London, 2010.